Available online at www.sciencedirect.com
SCIENCE DIRECT®
International Journal of Heat and Mass Transfer 49 (2006) 1516–1528
International Journal of HEAT and MASS TRANSFER
www.elsevier.com/locate/ijhmt

Pyramidal direct methanol fuel cells

S.M. Senn, D. Poulikakos *

Laboratory of Thermodynamics in Emerging Technologies, Department of Mechanical and Process Engineering, ETH Zurich, CH-8092 Zurich, Switzerland

Received 9 September 2004; received in revised form 16 March 2005
Available online 6 December 2005

Abstract

The main concept of this article is to allow for the optimized tree-like design of the flow distributors to actually define the shape of the fuel cell, thereby eliminating problems associated with the mismatch between a predecided rectangular shape and a functionally preferred channel distribution system. The work focuses on direct methanol fuel cells (DMFC). A one-dimensional across-the-cell model is extended to a two-dimensional along-the-channel model and numerically solved to predict the polarization curves of a direct methanol fuel cell with tree network channels and of a cell with traditional serpentine channels. For both flow configurations, pressure drop and pumping power are estimated. Net power densities are computed in terms of constructal parameters and operating conditions. In contrast to the traditional rectangular shape of fuel cells, the resulting ''pyramidal'' or ''double-staircase'' shape is based on the functionality of the fluid distribution system. It is found that tree network channels can provide substantially improved electric and net power densities compared to the traditional non-bifurcating single serpentine channels, as a result of their intrinsic advantage with respect to both mass transfer and pressure drop. For six (12) branching levels and inlet channel diameters of 0.05, 0.04, and 0.03 cm, the tree network channels allow for 14% (21%), 17% (26%), and 30% (46%) higher net power densities, respectively.

Keywords: Tree network channels; Constructal; Fractal tree-like; Fluid distributor; Direct methanol fuel cell

1. Introduction

In this article, constructal tree network channels introduced by Bejan [1–3] are investigated not only as a fluid distribution concept for the anode and cathode side of liquid-feed direct methanol fuel cells but also as a means to functionally define the shape of the fuel cells. A simple two-dimensional model is numerically solved to predict polarization curves, electric power density curves, and net power density curves of a direct methanol fuel cell with tree network channels as fluid distributors, and compare them to the respective curves of a cell with a traditional non-bifurcating serpentine channel. Variation of cell performance in terms of constructal and operating condition parameters is discussed and optima are identified. Characteristic variations along the channel of methanol and oxygen concentration, anode and cathode overpotential, and electric current density are discussed for both tree network channels and traditional non-bifurcating serpentine channels. Three-dimensional models [4] provide the most comprehensive and fundamental insight into the transport phenomena in fuel cells. However, their numerical solution still requires substantial computational time and resources, making them inappropriate for multiparametric optimization studies that usually require a large number of evaluations of an objective function. The functionality-optimized pyramidal fuel cell design was recently introduced by Senn and Poulikakos [5] with respect to hydrogen polymer electrolyte fuel cells, showing excellent promise compared to traditional alternatives. The fundamental characteristics of laminar mixing, heat transfer, and pressure drop in tree network channels were also investigated numerically [6],

* Corresponding author. Tel.: +41 1 632 2738; fax: +41 1 632 1176.
E-mail address: dimos.poulikakos@ethz.ch (D. Poulikakos).

0017-9310/$ - see front matter © 2005 Elsevier Ltd. All rights reserved.
doi:10.1016/j.ijheatmasstransfer.2005.08.034

Nomenclature

A	total cell area, cm^2
b	current collector width, cm
c^a	molar concentration of methanol, mol cm^{-3}
c^c	molar concentration of oxygen, mol cm^{-3}
D	diffusion coefficient, $cm^2\ s^{-1}$
E	electric power density, W cm^{-2}
F	Faraday constant, 96485 C mol^{-1}
h	channel width, cm
i_χ	exchange current density, A cm^{-3}
J	average cell current density, A cm^{-2}
j	local proton current density, A cm^{-2}
k	concentration factor
L	channel length, cm
l_b	backing layer thickness, cm
l_m	membrane thickness, cm
l_t	catalyst layer thickness, cm
N	molar flux, mol $cm^{-2}\ s^{-1}$
Nu	Nusselt number
n	total number of branching levels
n_d	drag coefficient
P	pumping power density, W cm^{-2}
p	pressure, Pa
Q	local rate of electrochemical reaction, A cm^{-3}
R	universal gas constant, 8.314 J K^{-1} mol^{-1}
Re	Reynolds number
Sh	Sherwood number
T	cell temperature, K
V_{cell}	cell potential, V
v	bulk velocity in the channel, cm s^{-1}
x	coordinate across the membrane, cm
y	coordinate, cm
z	coordinate along the channel, cm

Greek symbols

α	transfer coefficient
χ	number of turns in the serpentine channel
ε	effective porosity
ϕ	channel length ratio
φ	channel width ratio
γ	effective order of reaction
η	local overpotential in the catalyst layer, V
η_i	overpotential at the membrane/catalyst layer interface, V
η_{oc}	open-circuit potential, V
κ	mass transfer coefficient, cm s^{-1}
μ	dynamic viscosity, Pa s
Π	net power density, W cm^{-2}
σ	proton conductivity, Ω^{-1} cm^{-1}
ξ	loss coefficient

Subscripts

b	in the backing layer
h	in the channel
i	value at the membrane/catalyst layer interface
k	at the kth branching level
lim	limiting
m	in bulk membrane
max	maximum
ref	reference
s	stoichiometric
t	in the catalyst layer
w	water
0	at the zeroth branching level
χ	characteristic

Superscripts

a	on the anode side
c	on the cathode side

along with their application for thermal management in polymer electrolyte fuel cells. Vargas and Bejan [7] recently presented an elemental level thermodynamic optimization study for the electrodes of alkaline fuel cells. Entropy generation minimization [8] at the global level presents a major challenge in fuel cell research.

2. Mathematical formulation

A one-dimensional across-the-cell model originally developed and experimentally validated by Kulikovsky [9,10] is utilized to predict the polarization curves and the electric power density curves of a direct methanol fuel cell with tree network channels as fluid distributors. The original model [9,10] accounts for methanol and oxygen mass transfer through the backing layers, methanol permeation through the membrane, and non-uniform overpotential distributions across the finite-size catalyst layers. The model is extended to a two-dimensional model that additionally takes into account methanol and oxygen consumption along the channels, mass transfer between the channels and the backing layers, mass transfer in the lateral direction indicated by the y axis in Fig. 1, as well as overpotential variations along the channel. In addition, pressure drop and pumping power required for the fluid circulation are estimated considering also effects from bifurcations. Diffusion mass transport along the streamwise direction z (see Fig. 1) is neglected due to the high Peclet number. The

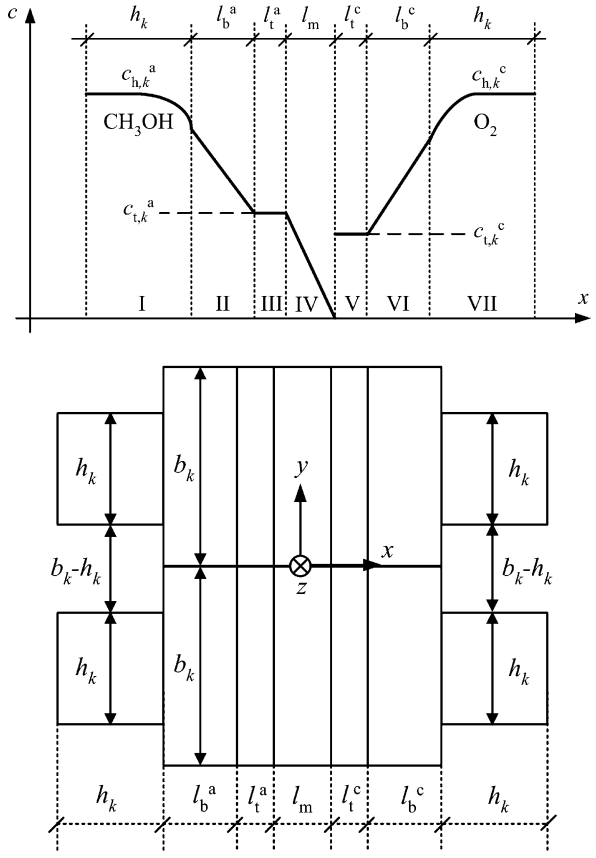

Fig. 1. Schematic drawing of methanol and oxygen concentration distributions across the cell, including anode channel (I), anode backing layer (II), anode catalyst layer (III), membrane (IV), cathode catalyst layer (V), cathode backing layer (VI), and cathode channel (VII).

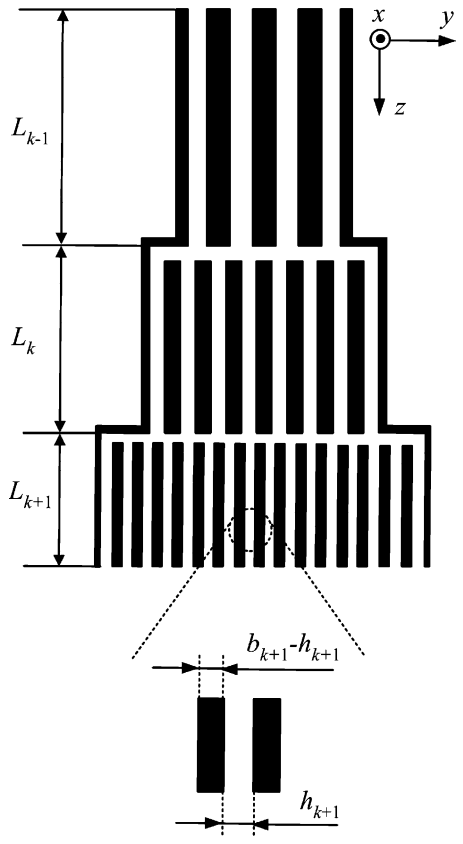

Fig. 2. Geometric structure of the pyramidal tree network fluid delivery system including channels (white) and current collector shoulders (black).

model is based on a variety of other assumptions [9,10]: Ohmic losses due to electron transport are neglected, thus a high electrical conductivity of the current collector plates, backing layers, and catalyst layers is assumed. Reactant concentrations are assumed to be constant across the finite-size catalyst layers. A constant diffusion coefficient of methanol is assumed inside the membrane. Methanol permeated through the membrane is assumed to completely react with oxygen in the cathode catalyst layer. The methanol concentration on the cathode side is assumed to be much smaller than the methanol concentration on the anode side. The electrolyte phase is assumed to be ideally hydrated and constant proton conductivities are assumed inside the membrane and the catalyst layers. The fluid velocity is assumed to remain constant along the channel of a certain branching level. The model is a single-phase one, two-phase flow [11,12] issues are not considered. Tafel-like expressions are used to predict the electrochemical reaction rates at the anode and cathode.

The geometric structure of a cell with tree network channels as fluid distributors on the anode and cathode side is outlined in Figs. 1 and 2. The anode tree network and the cathode tree network are identical and congruently superimposed. Schematic distributions of reactant concentrations across the cell are shown in Fig. 1. The white areas in Fig. 2 represent schematically the channels of the tree network having one inlet at the zeroth branching level and a number of 2^n outlets at the nth branching level, where n is the total number of branching levels. This means that the flow is subject to redistribute n times. Square cross-sectional channels of width h_k are considered, where the subscript k indicates the branching level. From the current collector width b_k, the current collector shoulder width $b_k - h_k$ follows. The backing layer thicknesses l_b^a and l_b^c, the catalyst layer thicknesses l_t^a and l_t^c, and the membrane thickness l_m are constant whereas h_k and b_k vary from one branching level to the next higher. The superscripts a and c refer to the anode and cathode side, respectively. The subscripts b, t, and m refer to the backing layer, the catalyst layer, and the membrane, respectively. It is assumed that at the interface between two consecutive branching levels, the flow is subject to redistribute uniformly to the channels of the higher branching level. This can be achieved with a gap of small flow resistance, for example. However, such manufacturing issues are not the main subject of this study. The aim of the present study is to investigate the fundamental mass transfer and fluid dynamics aspects of the problem. The model is based on first principles and it is chosen for its effectiveness if one takes into account its simplicity.

2.1. Governing equations: branching level k

In direct methanol fuel cells, methanol and water are converted to carbon dioxide and protons at the anode, according to

$$CH_3OH + H_2O \rightarrow CO_2 + 6H^+ + 6e^-. \quad (1)$$

Protons are transported through the electrolyte phase of the catalyst layers and the membrane to react with oxygen in the cathode catalyst layer, according to

$$O_2 + 4H^+ + 4e^- \rightarrow 2H_2O. \quad (2)$$

In this study, the case where dry air is fed on the cathode side is considered. A constant channel width ratio φ between two consecutive branching levels is imposed, such that the channel width at the kth branching level h_k can be related to the channel width at the zeroth branching level h_0 as

$$h_k = h_0\varphi^k, \quad (3)$$

where $h_{k+1} = h_k\varphi$. The current collector width scales identically and

$$b_k = b_0\varphi^k \quad (4)$$

holds, where $b_{k+1} = b_k\varphi$. The constant length ratio ϕ relates the channel length at the kth branching level, given by

$$L_k = L_0\phi^k, \quad (5)$$

to the channel length at the zeroth branching level L_0, where $L_{k+1} = L_k\phi$. It is assumed that the number of channels increases by a factor of two from one branching level to the next higher. A mass balance at the interface between two consecutive branching levels then leads to

$$v_k^a h_k^2 = 2v_{k+1}^a h_{k+1}^2, \quad (6)$$

where v_k^a represents the bulk velocity in an anode channel of the kth branching level that can be expressed in terms of the anode inlet velocity v_0^a at the zeroth branching level, given by

$$v_k^a = 2^{-k}\varphi^{-2k}v_0^a. \quad (7)$$

In this study, $\varphi = 2^{-1/3}$ is assumed and therefore the fluid velocity is subject to decrease by a factor of $2^{-1}\varphi^{-2} \approx 0.79$ from one branching level to the next higher branching level. Replacing the superscript a by c in Eqs. (6) and (7) leads to analogous relations on the cathode side. Herein, it is implicitly assumed that the bulk velocities are constant along the channels of a certain branching level, that is, $v_k^a = \text{const.}$ and $v_k^c = \text{const.}$ Conservation of electric current in the anode catalyst layer is formulated as

$$\frac{\partial j_k}{\partial x_k} = Q_k^a, \quad (8)$$

where j_k is the local proton current density in the catalyst layer, x_k is the across-the-cell coordinate, and Q_k^a is the volumetric transfer current density. Ohm's law relates the local current density to the local electric field through the catalyst layer proton conductivity σ_t^a, that is

$$j_k = \sigma_t^a \frac{\partial \eta_k^a}{\partial x_k}, \quad (9)$$

where the anode overpotential η_k^a substitutes the local electrolyte phase potential. Note that η_k^a is defined as the difference between the solid phase potential and the local electrolyte phase potential, where the solid phase potential is assumed to be constant. The volumetric transfer current density can be written as

$$Q_k^a = i_\chi^a \left(\frac{c_{t,k}^a}{c_{ref}^a}\right)^{\gamma^a} \exp\left(\frac{\alpha^a F}{RT}\eta_k^a\right), \quad (10)$$

where i_χ^a is the exchange current density, $c_{t,k}^a$ is the methanol concentration in the anode catalyst layer, c_{ref}^a is the reference concentration, γ^a is the reaction order, α^a is the transfer coefficient, F is the Faraday constant, R is the universal gas constant, and T is the temperature. Identical relations can be formulated for the cathode catalyst layer, that is

$$\frac{\partial j_k}{\partial x_k} = -Q_k^c, \quad (11)$$

$$j_k = -\sigma_t^c \frac{\partial \eta_k^c}{\partial x_k}, \quad (12)$$

and

$$Q_k^c = i_\chi^c \left(\frac{c_{t,k}^c}{c_{ref}^c}\right)^{\gamma^c} \exp\left(\frac{\alpha^c F}{RT}\eta_k^c\right), \quad (13)$$

where $c_{t,k}^c$ is the oxygen concentration in the cathode catalyst layer. Note that the local cathode overpotential η_k^c is defined as the difference between the local electrolyte phase potential and the solid phase potential, where the latter is assumed to be constant. The flux of methanol mass transfer from the bulk fluid flow in the channel to the catalyst layer can be written as

$$\frac{c_{h,k}^a - c_{t,k}^a}{(\kappa_{h,k}^a)^{-1} + (\kappa_{b,k}^a)^{-1}} = \frac{j_{i,k}}{6F} + N_k, \quad (14)$$

where $c_{h,k}^a$ is the mean molar concentration of methanol in the anode channel (the subscript h refers to the channel), $\kappa_{h,k}^a$ is the mass transfer coefficient between the bulk fluid flow and the channel/backing layer interface, $\kappa_{b,k}^a$ is the mass transfer coefficient between the channel/backing layer interface and the catalyst layer, $j_{i,k}$ is the value of the local proton current density at the membrane/catalyst layer interface (the subscript i refers to the membrane/catalyst layer interface), and

$$N_k = \frac{D_m c_{t,k}^a}{l_m} + n_d \frac{j_{i,k}}{F}\frac{c_{t,k}^a}{w^a} \quad (15)$$

denotes the flux of methanol through the membrane. Herein, D_m is the diffusion coefficient of methanol in the membrane, n_d is a drag coefficient that defines the number of methanol molecules transported through the membrane by one proton, and w^a is the water concentration on the

anode side. In the first term on the right-hand side of Eq. (15) it is assumed that the methanol concentration in the cathode catalyst layer is much smaller than in the anode catalyst layer. Similarly, the flux of oxygen mass transfer from the bulk fluid flow in the channel to the cathode catalyst layer can be formulated as

$$\frac{c^{c}_{h,k}-c^{c}_{t,k}}{(\kappa^{c}_{h,k})^{-1}+(\kappa^{c}_{b,k})^{-1}}=\frac{j_{i,k}}{4F}+\frac{3}{2}N_k, \tag{16}$$

where $c^{c}_{h,k}$ is the mean oxygen concentration in the cathode channel. It is assumed that methanol transported through the membrane completely reacts with oxygen in the cathode catalyst layer, according to

$$2CH_3OH+3O_2\rightarrow 2CO_2+4H_2O. \tag{17}$$

For laminar fully developed flow in a square duct with three adiabatic walls and a wall with a uniform heat flux, the Nusselt number Nu is constant, that is, $Nu=2.712$ (see Ref. [13]). The Sherwood number Sh can be related to the Nusselt number Nu according to the Reynolds analogy [14,15], $Sh=NuLe$, where $Le=Sc/Pr$ is the Lewis number, Sc is the Schmidt number, and Pr is the Prandtl number. For dry air that is fed on the cathode side, $Le\approx 1$ applies. For the liquid that is fed on the anode side, the Chilton–Colburn analogy [14,15], $Sh=Nu\ Le(Pr/Sc)^{2/3}$, suggests that the Sherwood number and the Nusselt number are of the same order of magnitude in this study. In order to remain consistent in accuracy, $Sh/Nu=1$ is assumed in this analysis. The Sherwood number for mass transfer between the bulk fluid flow in the channel and the channel/backing layer interface is given then by

$$Sh^{a}_{h}=2.7, \tag{18}$$

and the corresponding mass transfer coefficient at the kth branching level reads

$$\kappa^{a}_{h,k}=Sh^{a}_{h}D^{a}_{h}/h_k, \tag{19}$$

where D^{a}_{h} denotes the methanol diffusion coefficient in the anode channel. The Sherwood number for mass transfer between the channel/backing layer interface and the catalyst layer shall be empirically defined as

$$Sh^{a}_{b,k}=[1+(b_k-h_k)/(4l^{a}_{b})]^{-1}. \tag{20}$$

The corresponding mass transfer coefficient at the kth branching level reads

$$\kappa^{a}_{b,k}=\frac{Sh^{a}_{b,k}D^{a}_{b}}{l^{a}_{b}}=\frac{D^{a}_{b}}{\{l^{a}_{b}+[l^{a}_{b}+(b_k-h_k)/2]\}/2}, \tag{21}$$

where D^{a}_{b} is the effective methanol diffusion coefficient in the anode backing layer. The effective diffusion length scale in Eq. (21), denoted by the denominator, is defined as the mean value between a minimum diffusion length l^{a}_{b} and a maximum diffusion length $l^{a}_{b}+(b_k-h_k)/2$ between the channel/backing layer interface and the catalyst layer (see Fig. 1). In a previous study [5], three-dimensional solutions of the Navier–Stokes and species conservation equations showed that the mass transfer correlation given in Eq. (20) is a good approximation for low-diameter channels and $b_k=2h_k$. The Bruggeman correction [16,17] relates the free-stream diffusion coefficient D^{a}_{h} to the effective diffusion coefficient D^{a}_{b} through the backing layer porosity ε, according to

$$D^{a}_{b}=D^{a}_{h}\varepsilon^{3/2} \tag{22}$$

with a tortuosity factor of 3/2. Similar relations hold on the cathode side and can be written as

$$Sh^{c}_{h}=2.7, \tag{23}$$

$$\kappa^{c}_{h,k}=Sh^{c}_{h}D^{c}_{h}/h_k, \tag{24}$$

$$Sh^{c}_{b,k}=[1+(b_k-h_k)/(4l^{c}_{b})]^{-1}, \tag{25}$$

$$\kappa^{c}_{b,k}=\frac{Sh^{c}_{b,k}D^{c}_{b}}{l^{c}_{b}}=\frac{D^{c}_{b}}{\{l^{c}_{b}+[l^{c}_{b}+(b_k-h_k)/2]\}/2}, \tag{26}$$

and

$$D^{c}_{b}=D^{c}_{h}\varepsilon^{3/2}. \tag{27}$$

From Eqs. (8)–(10) and Eqs. (14) and (15) a simple relation between the local anode overpotential $\eta^{a}_{i,k}$ and the local proton current density $j_{i,k}$, both evaluated at the membrane/anode catalyst layer interface, can be obtained [9,10]:

$$j_{i,k}/j^{a}_{\chi}=X^{a}_{k}\tan X^{a}_{k}, \tag{28}$$

where

$$X^{a}_{k}=\left[k^{a}_{k}\exp\left(\frac{\eta^{a}_{i,k}}{\eta^{a}_{\chi}}\right)\left(1-\frac{j_{i,k}}{j^{a}_{lim,k}}\right)^{\gamma^{a}}\times\left(1+\beta_k+n_d\frac{j_{i,k}}{j_{w,k}}\right)^{-\gamma^{a}}-\left(\frac{j_{i,k}}{j^{a}_{\chi}}\right)^{2}\right]^{1/2}, \tag{29}$$

$$\eta^{a}_{\chi}=\frac{RT}{\alpha^{a}F},\quad j^{a}_{\chi}=\frac{2\sigma^{a}_{t}\eta^{a}_{\chi}}{l^{a}_{t}}, \tag{30}$$

$$k^{a}_{k}=\frac{l^{a}_{t}i^{a}_{\chi}}{j^{a}_{\chi}}\left(\frac{c^{a}_{h,k}}{c^{a}_{ref}}\right)^{\gamma^{a}}, \tag{31}$$

$$j^{a}_{lim,k}=6F\frac{c^{a}_{h,k}}{(\kappa^{a}_{h,k})^{-1}+(\kappa^{a}_{b,k})^{-1}}, \tag{32}$$

$$\beta_k=\frac{D_m}{l_m}[(\kappa^{a}_{h,k})^{-1}+(\kappa^{a}_{b,k})^{-1}], \tag{33}$$

$$j_{w,k}=F\frac{w^{a}}{(\kappa^{a}_{h,k})^{-1}+(\kappa^{a}_{b,k})^{-1}}, \tag{34}$$

and

$$N_k=\frac{j^{a}_{lim,k}}{6F}\left(\frac{\beta_k+n_d j_{i,k}/j_{w,k}}{1+\beta_k+n_d j_{i,k}/j_{w,k}}\right)\times(1-j_{i,k}/j^{a}_{lim,k}). \tag{35}$$

A detailed derivation of Eq. (28) is given by Kulikovsky [9,10]. From Eqs. (11)–(16) a simple relation between the local cathode overpotential $\eta^{c}_{i,k}$ and the local proton current density $j_{i,k}$, both evaluated at the membrane/cathode catalyst layer interface, can be obtained [9,10]:

$$j_{i,k}/j_\chi^c = X_k^c \tan X_k^c, \tag{36}$$

where

$$X_k^c = \left[k_k^c \exp\left(\frac{\eta_{i,k}^c}{\eta_\chi^c}\right)\left(1 - \frac{j_{i,k}}{j_{\lim,k}^c} - r_k\right)^{\gamma^c} - \left(\frac{j_{i,k}}{j_\chi^c}\right)^2 \right]^{1/2}, \tag{37}$$

$$\eta_\chi^c = \frac{RT}{\alpha^c F}, \quad j_\chi^c = \frac{2\sigma_t^c \eta_\chi^c}{l_t^c}, \tag{38}$$

$$k_k^c = \frac{l_t^c i_\chi^c}{j_\chi^c}\left(\frac{c_{h,k}^c}{c_{ref}^c}\right)^{\gamma^c}, \tag{39}$$

$$j_{\lim,k}^c = 4F\frac{c_{h,k}^c}{(\kappa_{h,k}^c)^{-1} + (\kappa_{b,k}^c)^{-1}}, \tag{40}$$

and

$$r_k = \frac{j_{\lim,k}^a}{j_{\lim,k}^c}\left(\frac{\beta_k + n_d j_{i,k}/j_{w,k}}{1 + \beta_k + n_d j_{i,k}/j_{w,k}}\right)(1 - j_{i,k}/j_{\lim,k}^a). \tag{41}$$

The derivation of Eq. (36) is given by Kulikovsky [9,10]. Note that Eq. (36) is formulated at a certain position z_k. The latter is the coordinate along the flow direction, it is zero at the beginning of branching level k, and equals L_k at the end of branching level k. Mass conservation of methanol and oxygen along the channel reads

$$\frac{d(c_{h,k}^a/c_{h,k}^a(z_k=0))}{d(z_k/L_k)} = -\frac{j_{i,k}}{j_{s,k}^a} - 6F\frac{N_k}{j_{s,k}^a}, \tag{42}$$

and

$$\frac{d(c_{h,k}^c/c_{h,k}^c(z_k=0))}{d(z_k/L_k)} = -\frac{j_{i,k}}{j_{s,k}^c} - 6F\frac{N_k}{j_{s,k}^c}, \tag{43}$$

respectively. Herein, the quantities

$$j_{s,k}^a = 6F\frac{h_k^2 v_k^a c_{h,k}^a(z_k=0)}{b_k L_k}, \tag{44}$$

and

$$j_{s,k}^c = 4F\frac{h_k^2 v_k^c c_{h,k}^c(z_k=0)}{b_k L_k} \tag{45}$$

represent the stoichiometric current densities of the kth branching level on the anode and cathode side, respectively. They are related to the cell stoichiometric current densities j_s^a and j_s^c as

$$j_s^a = j_{s,0}^a \frac{1}{\sum_{k=0}^n \phi^k \varphi^k 2^k}, \tag{46}$$

and

$$j_s^c = j_{s,0}^c \frac{1}{\sum_{k=0}^n \phi^k \varphi^k 2^k}, \tag{47}$$

respectively, where $j_s^a = j_{s,0}^a b_0 L_0/A$ and $j_s^c = j_{s,0}^c b_0 L_0/A$ further applies. In Eqs. (42) and (43) it is assumed that the bulk velocities are constant along the channels of a certain branching level, that is, $v_k^a = \text{const.}$ and $v_k^c = \text{const.}$ Diffusion mass transport along the streamwise direction z_k is neglected due to the high Peclet numbers $Pe_k^a = v_k^a L_k/D_h^a$ and $Pe_k^c = v_k^c L_k/D_h^c$ in this study. Averaging the local current density $j_{i,k}$ along the channel yields an average current density of the kth branching level, given by

$$\bar{j}_{i,k} = L_k^{-1}\int_0^{L_k} j_{i,k}\,dz_k. \tag{48}$$

2.2. Governing equations: tree network

The model describing the transport phenomena at a certain branching level k, as discussed in the last subsection, is used to predict the current–voltage behavior of a cell with an entire tree network channel system including n branching levels. The average cell current density can then be written as

$$J = A^{-1}\sum_{k=0}^n \bar{j}_{i,k} L_k b_k 2^k, \tag{49}$$

where

$$A = \sum_{k=0}^n L_k b_k 2^k \tag{50}$$

is the total cell area. The factor $L_k b_k 2^k$ in Eq. (49) represents the cell area that belongs to the kth branching level. If the cell potential V_{cell} is constant along the tree network channels, then J and V_{cell} describe the current–voltage behavior of a cell with tree network fluid distributors on the anode and cathode side.

2.3. Pressure drop and pumping power

Electrochemical reaction rates depend on local reactant concentrations. Since the reactant concentrations decrease downstream the channels, the local current density also decreases along the flow direction. The higher the fluid inlet velocities, the lower the relative reduction in reactant concentrations along the channels is, for a constant cell potential. In the limiting case where the inlet velocities tend to infinity, the reactant concentrations remain constant along the flow direction and the average cell current density corresponds to the local current density at the inlet. Hence, the electric power density can be enhanced by increasing the anode and cathode inlet flow rates or the stoichiometric flow ratios, however, the pumping power required for the fluid circulation is increased at the same time. If a considerable amount of electric power is required for pumping power, the net power available to the user can be substantially reduced, implying reduced overall fuel cell efficiency. Consequently, there exists a thermodynamic optimum in this context. For the optimization of the fluid distribution system of direct methanol fuel cells, it is therefore imperative that pressure drop be considered as a loss mechanism.

The pressure drop in the tree network channels can be estimated by assuming geometrically similar shapes of

channel cross sections. On the anode side, the overall pressure drop can be written as

$$\Delta p^{\mathrm{a}} = \sum_{k=0}^{n} C^{\mathrm{a}} \frac{L_k v_k^{\mathrm{a}}}{h_k^2} + \sum_{k=0}^{n-1} \xi \rho^{\mathrm{a}} (v_k^{\mathrm{a}})^2/2, \quad \text{if } n \geqslant 1, \tag{51}$$

or

$$\Delta p^{\mathrm{a}} = C^{\mathrm{a}} \frac{L_0 v_0^{\mathrm{a}}}{h_0^2} \frac{1-\phi^{n+1}/(2^{n+1}\varphi^{4(n+1)})}{1-\phi/(2\varphi^4)} + \frac{\xi \rho^{\mathrm{a}} (v_0^{\mathrm{a}})^2}{2} \frac{1-(4\varphi^4)^{-n}}{1-(4\varphi^4)^{-1}}, \quad \text{if } n \geqslant 1, \tag{52}$$

and

$$\Delta p^{\mathrm{a}} = C^{\mathrm{a}} \frac{L_0 v_0^{\mathrm{a}}}{h_0^2} + \frac{\chi \xi \rho^{\mathrm{a}} (v_0^{\mathrm{a}})^2}{2}, \quad \text{if } n = 0, \tag{53}$$

where $n = 0$ *indicates a tree network with zero branching levels which essentially corresponds to a single non-bifurcating channel, representing a traditional serpentine fluid delivery system*. The resistance coefficient ξ accounts for the pressure drop due to bifurcations in the tree network. An identical resistance coefficient ξ is assumed to account for the pressure drop due to turns in the traditional non-bifurcating channel. The factor χ indicates the number of turns and ρ^{a} is the fluid density. The coefficient C^{a} is given as

$$C^{\mathrm{a}} = \mu^{\mathrm{a}} fRe/2, \tag{54}$$

where the friction factor for a square cross-sectional channel under fully developed flow conditions is given as $fRe \approx 56.9$ (see Ref. [13]). The pumping power density on the anode side, defined as pumping power per cell area A, is given then as

$$P^{\mathrm{a}} = h_0^2 v_0^{\mathrm{a}} \Delta p^{\mathrm{a}} A^{-1}, \tag{55}$$

where $h_0^2 v_0^{\mathrm{a}}$ is the volumetric inlet flow rate on the anode side. Replacing the superscript a by c in Eqs. (51)–(55) leads to the pumping power density P^{c} on the cathode side.

2.4. Electric and net power density

The cell potential V_{cell} is obtained by subtracting the main voltage losses, that is, the anode overpotential, the cathode overpotential, and the membrane potential loss, from the open-circuit potential η_{oc}, and may be written as

$$\frac{V_{\mathrm{cell}}}{\eta_{\mathrm{oc}}} = 1 - \frac{\eta_{\mathrm{i},k}^{\mathrm{a}}}{\eta_{\chi}^{\mathrm{a}}} \frac{\eta_{\chi}^{\mathrm{a}}}{\eta_{\mathrm{oc}}} - \frac{\eta_{\mathrm{i},k}^{\mathrm{c}}}{\eta_{\chi}^{\mathrm{c}}} \frac{\eta_{\chi}^{\mathrm{c}}}{\eta_{\mathrm{oc}}} - \frac{j_{\mathrm{i},k}}{j_{\mathrm{m}}} \tag{56}$$

with $j_{\mathrm{m}} = \sigma_{\mathrm{m}} \eta_{\mathrm{oc}}/l_{\mathrm{m}}$, where σ_{m} is the proton conductivity in the membrane and l_{m} is the membrane thickness. The electric power density E of the cell, defined as the total electric power per cell area A, is given then as

$$E = JV_{\mathrm{cell}}. \tag{57}$$

Finally, a net power density

$$\Pi = E - P^{\mathrm{a}} - P^{\mathrm{c}} \tag{58}$$

can be defined as the difference between the electric power density and the power density required for fluid circulation on the anode and cathode sides.

3. Solution method

The model is solved numerically along the tree network. The methanol concentration at the anode inlet, the oxygen concentration at the cathode inlet, and the cell potential V_{cell} are prescribed first. The equations governing transport in the across-the-cell direction x_k are then solved numerically. Herein, the local proton current density $j_{\mathrm{i},k}$ at the membrane/catalyst layer interface is first estimated, based on which the anode overpotential $\eta_{\mathrm{i},k}^{\mathrm{a}}$ and the cathode overpotential $\eta_{\mathrm{i},k}^{\mathrm{c}}$ can be numerically obtained through Eqs. (28) and (36), respectively, using the secant method. The resulting cell potential can then be calculated from Eq. (56). If it does not coincide with the prescribed cell potential, then a new value for $j_{i,k}$ is estimated and the previous steps are repeated until convergence is achieved. This outer iteration loop is addressed again with the secant method. The initial value problem given by Eqs. (42) and (43) is numerically solved with a standard Runge–Kutta method, where the just described across-the-cell procedure is repeated at each integration step. The numerical solution converges very quickly due to the fourth order error of the Runge–Kutta method.

4. Results and discussion

In this section, the effect of geometric and operating parameter variations on the polarization curve, the electric power density curve, and the net power density curve is discussed. In addition, the characteristic variations along the tree network of methanol and oxygen concentration, anode and cathode overpotential, and current density are compared to the respective characteristics of a single non-bifurcating channel. A constant cell area A is considered for both flow distribution systems. The numerical results are based on the parameters listed in Table 1.

4.1. Concentration variation along the channels

The variation of the methanol concentration $c_{\mathrm{h},k}^{\mathrm{a}}$ and the oxygen concentration $c_{\mathrm{h},k}^{\mathrm{c}}$ along the channels of a tree network with $n = 6$ number of branching levels is shown in Fig. 3(a) for different anode inlet velocities v_0^{a} and cathode inlet velocities v_0^{c}. The inlet Reynolds numbers on the anode and cathode side are defined as $Re_0^{\mathrm{a}} = \rho^{\mathrm{a}} v_0^{\mathrm{a}} h_0/\mu^{\mathrm{a}}$ and $Re_0^{\mathrm{c}} = \rho^{\mathrm{c}} v_0^{\mathrm{c}} h_0/\mu^{\mathrm{c}}$, respectively. Labels indicate values of v_0^{c} where $v_0^{\mathrm{a}} = 0.02 v_0^{\mathrm{c}}/5$. Note that the along-the-channel coordinate z is defined as $z = z_k + L_{k-1} + L_{k-2} + \cdots + L_0$ and that the total length L is defined as $L = L_0 + L_1 + L_2 + \cdots + L_n$, such that $z/L = 0$ and $z/L = 1$ refer to the inlet and outlets of the tree network, respectively. Concentration variations along a single non-bifurcating channel covering the same cell area A are shown in Fig. 3(b) for different inlet velocities. The two graphs indicate how the characteristic concentration profiles along the tree network fundamentally differ from the characteristic concentration profiles along a single non-bifurcating channel. In the tree network channels, the reactant concentrations

Table 1
Parameters

Cell temperature T (K)	363[d]
Anode pressure level p^a (bar)	1[d]
Cathode pressure level p^c (bar)	1[e]
Open-circuit potential η_{oc} (V)	1.21
Membrane thickness l_m (cm)	0.0206[d]
Anode catalyst layer thickness l_t^a (cm)	0.0015[d]
Cathode catalyst layer thickness l_t^c (cm)	0.005[d]
Backing layer thickness l_b^a, l_b^c (cm)	0.03[d]
Membrane proton conductivity σ_m (Ω^{-1} cm^{-1})	0.1[d]
Catalyst layer proton conductivity σ_t(Ω^{-1} cm^{-1})	0.01[d]
Reference molar concentration c_{ref}^a (mol cm^{-3})	1.0×10^{-3}[d]
Reference molar concentration c_{ref}^c (mol cm^{-3})	3.2×10^{-5}[d]
Anode exchange current density i_χ^a (A cm^{-3})	1.1×10^{-2}[d]
Cathode exchange current density i_χ^c (A cm^{-3})	1.1×10^{-2}[d]
Effective order of anode reaction γ^a	0.5[d]
Effective order of cathode reaction γ^c	1[d]
Anode transfer coefficient α^a	0.8[d]
Cathode transfer coefficient α^c	0.7[d]
Backing layer effective porosity ε	0.2[e]
Dynamic viscosity μ^a (Pa s)	3.2×10^{-4}[f]
Dynamic viscosity μ^c (Pa s)	2.1×10^{-5}[f]
Loss coefficient ξ	1.0[g]
Drag coefficient n_d	1.0[d]
Inlet methanol concentration $c_{h,0}^a(0)$ (mol cm^{-3})	1.5×10^{-3}[e]
Inlet oxygen concentration $c_{h,0}^c(0)$ (mol cm^{-3})	6.96×10^{-6}
Total flow-field area A (cm^2)	9[d,h]
Diffusion coefficient of methanol	
in the channel D_h^a (cm^2 s^{-1})	2.0×10^{-4}[i]
in the anode backing layer D_b^a (cm^2 s^{-1})	1.8×10^{-5}[d]
in the membrane D_m (cm^2 s^{-1})	1.0×10^{-5}[d]
Diffusion coefficient of oxygen	
in the channel D_h^c (cm^2 s^{-1})	0.29[j]
in the cathode backing layer D_b^c (cm^2 s^{-1})	2.6×10^{-2}[k]

[d] Ref. [9].
[e] Assumed.
[f] Ref. [19].
[g] Ref. [20].
[h] Ref. [21].
[i] Obtained through Eq. (22).
[j] Ref. [14].
[k] Obtained through Eq. (27).

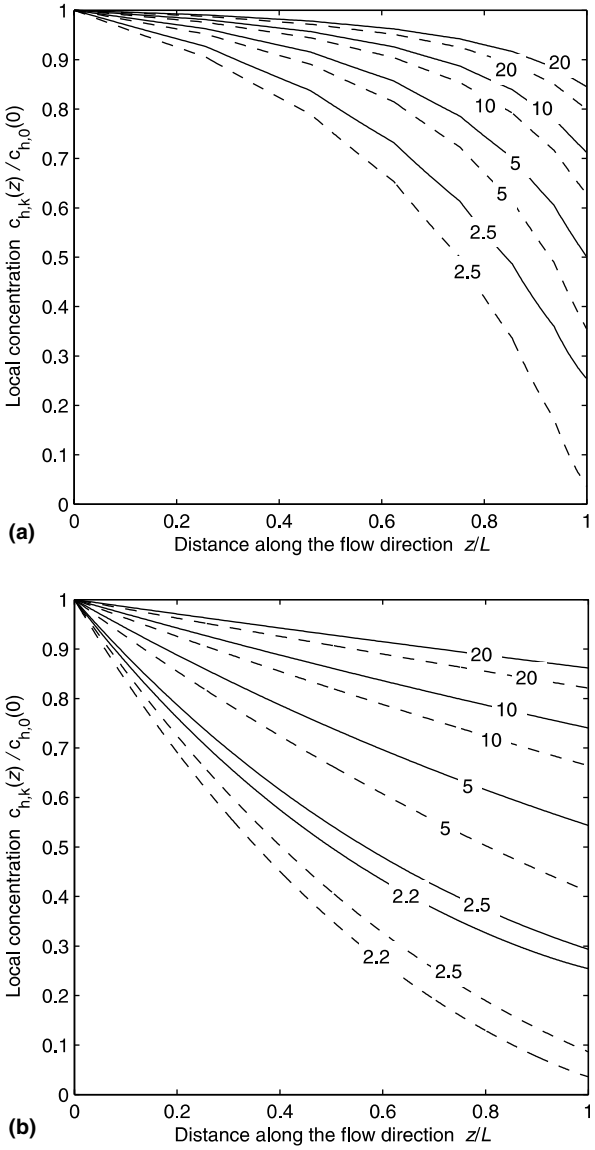

Fig. 3. Variation of the methanol concentration $c_{h,k}^a$ (solid lines) and the oxygen concentration $c_{h,k}^c$ (dashed lines) along the flow direction for different inlet velocities v_0^a and v_0^c (i.e., $v_0^a = (0.01, 0.02, 0.04, 0.08)$ m/s and $v_0^c = (2.5, 5, 10, 20)$ m/s) corresponding to $Re_0^a = (15, 30, 60, 120)$ and $Re_0^c = (57, 115, 229, 459)$, with $b_0 = 0.1$ cm, $h_0 = 0.05$ cm, and $V_{cell} = 0.3$ V. Labels indicate values of v_0^c where $v_0^a = 0.01v_0^c/2.5$. (a) Tree network fluid distributor with $n = 6$, $\varphi = 2^{-1/3}$, and $\phi = 2^{-1/3}$. (b) Traditional fluid distributor.

decay faster towards the outlets than near the inlet (see Fig. 3(a)). The opposite is the case for the non-bifurcating channel (see Fig. 3(b)). The characteristic concentration profiles along a single branching level reflect the characteristics of a traditional channel, whereas the sequence of profiles including more than one branching level has a different characteristic. This fundamental difference is due the fact that the channel cross section and the Reynolds number decrease in the tree network from one branching level to the next higher. The Reynolds numbers of consecutive branching levels are related as $Re_{k+1}/Re_k = 1/(2\varphi)$. For a channel width ratio $\varphi = 2^{-1/3}$, $Re_{k+1}/Re_k \approx 0.63$ results.

4.2. Current density variation along the channels

The variation of the local current density along the channels is shown in Fig. 4 for both flow configurations and different inlet flow rates. For the tree network, local discontinuities appear at the interface between two consecutive branching levels, since the geometric details of the transition are not taken into account and a sudden change in channel width is considered. The lower the inlet flow rates, the more the local current density decays along the tree network. For low inlet flow rates the distribution of the local current density has its maximum at the inlet. For high inlet flow rates, the maximum of the local current density distribution is shifted downstream the channels. It should be noted that if the inlet flow rates tend to infinity, the variation of the local current density along the tree net-

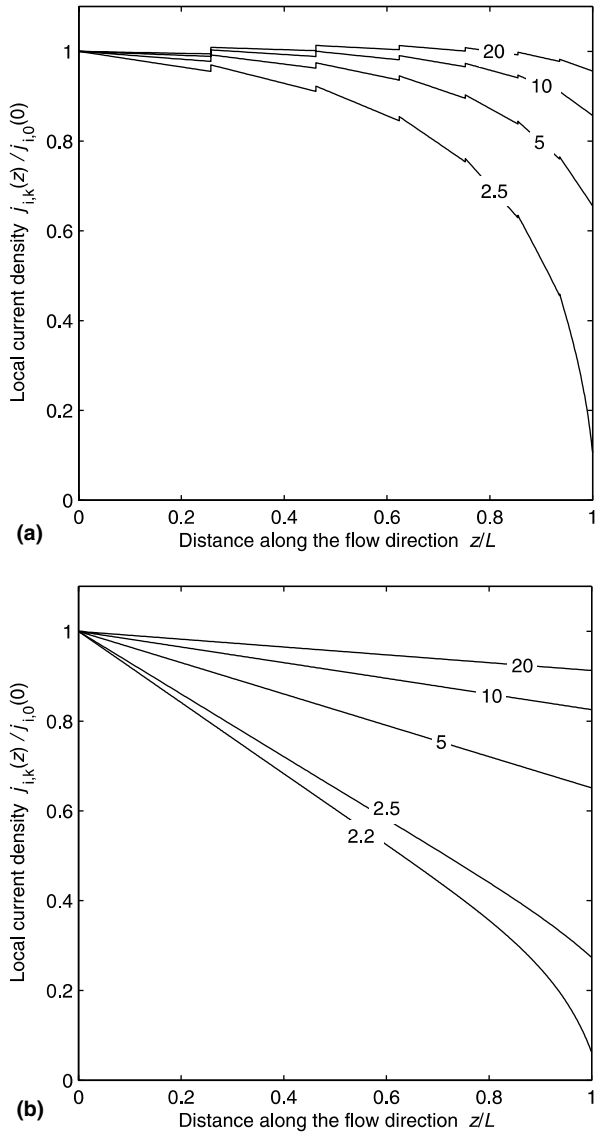

Fig. 4. Variation of the current density $j_{i,k}$ along the flow direction for different inlet velocities v_0^a and v_0^c (i.e., $v_0^a = (0.01, 0.02, 0.04, 0.08)$ m/s and $v_0^c = (2.5, 5, 10, 20)$ m/s) with $b_0 = 0.1$ cm, $h_0 = 0.05$ cm, and $V_{cell} = 0.3$ V. Labels indicate values of v_0^c where $v_0^a = 0.01 v_0^c/2.5$. (a) Tree network fluid distributor with $n = 6$, $\varphi = 2^{-1/3}$, and $\phi = 2^{-1/3}$. (b) Traditional fluid distributor.

work is described by a right-angled monotonically increasing staircase-shaped "curve" with its maximum near the outlet. The term "staircase-shaped" or "pyramidal" as part of the name of the herein proposed fuel cell fluid distribution concept refers in fact not only to the geometric structure but also to the intrinsic nature of the entire transport phenomena. The variation of the local current density along the tree network is shown in Fig. 5 for different numbers of branching levels n.

4.3. Electric and net power densities

The polarization curves of a cell with tree network channels as fluid distributors are shown in Fig. 6(a) for different

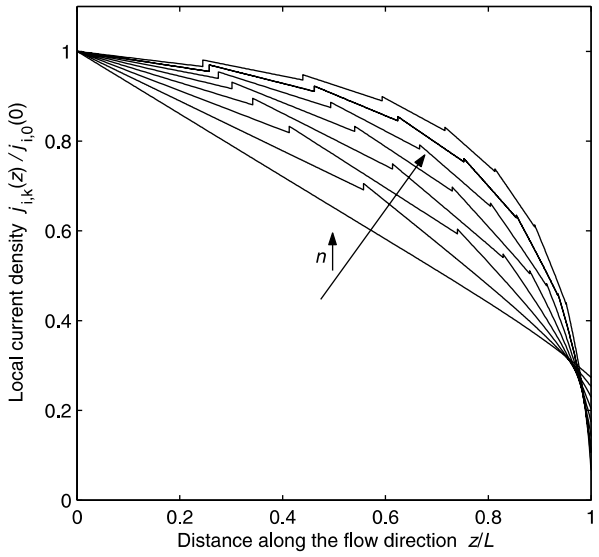

Fig. 5. Variation of the local current density $j_{i,k}$ along the flow direction for different numbers of branching levels n [i.e., $n = (0, 1, 2, 3, \ldots, 7)$] with $v_0^a = 0.01$ m/s, $v_0^c = 2.5$ m/s, $b_0 = 0.1$ cm, $h_0 = 0.05$ cm, $\varphi = 2^{-1/3}$, $\phi = 2^{-1/3}$, and $V_{cell} = 0.3$ V.

inlet flow rates, together with the polarization curves of a cell with a single non-bifurcating channel. If the flow rate is increased, the high current density end of the polarization curve is shifted to the right, that is, the limiting current density is increased, approaching asymptotically a maximum limiting current density at infinite inlet flow rates. It can be seen that for a constant cell potential the tree network channels provide higher cell current densities than the traditional channels. The corresponding electric power density curves are plotted in Fig. 6(b). For inlet velocities v_0^c of 5, 10, 20, 30, 50, and ∞ m/s, it is seen that compared to the traditional system, the tree network system provides 3.9%, 4.9%, 5.3%, 5.4%, 5.5%, and 5.5% higher maximum electric power densities, respectively. Herein, the maxima of the electric power density curves are compared. The net power density curves are shown in Fig. 6(c). For inlet velocities v_0^c of 5, 10, 20, and 30 m/s, it is seen that compared to the traditional system, the tree network system provides 6.3%, 14%, 59%, and 8.4×10^2% higher maximum net power densities, respectively. For $n = 9$, this last sequence reads 7.7%, 17%, 69%, and 1.2×10^3% (see Fig. 7(a)). For $n = 12$, the sequence reads 8.3%, 19%, 77%, and 1.9×10^3% (see Fig. 7(b)). For $n = 15$, the sequence reads 8.7%, 21%, 83%, and 3.2×10^3% (see Fig. 7(c)).

4.4. Maximum electric and net power densities

A fixed geometry of a tree network channel system shall be considered first, for which the net power density is to be optimized in terms of two optimization parameters: the inlet flow rate and the average cell current density. From Fig. 6(c) it can be seen that there exists an optimum pair, that is, an optimum inlet flow rate and an optimum average

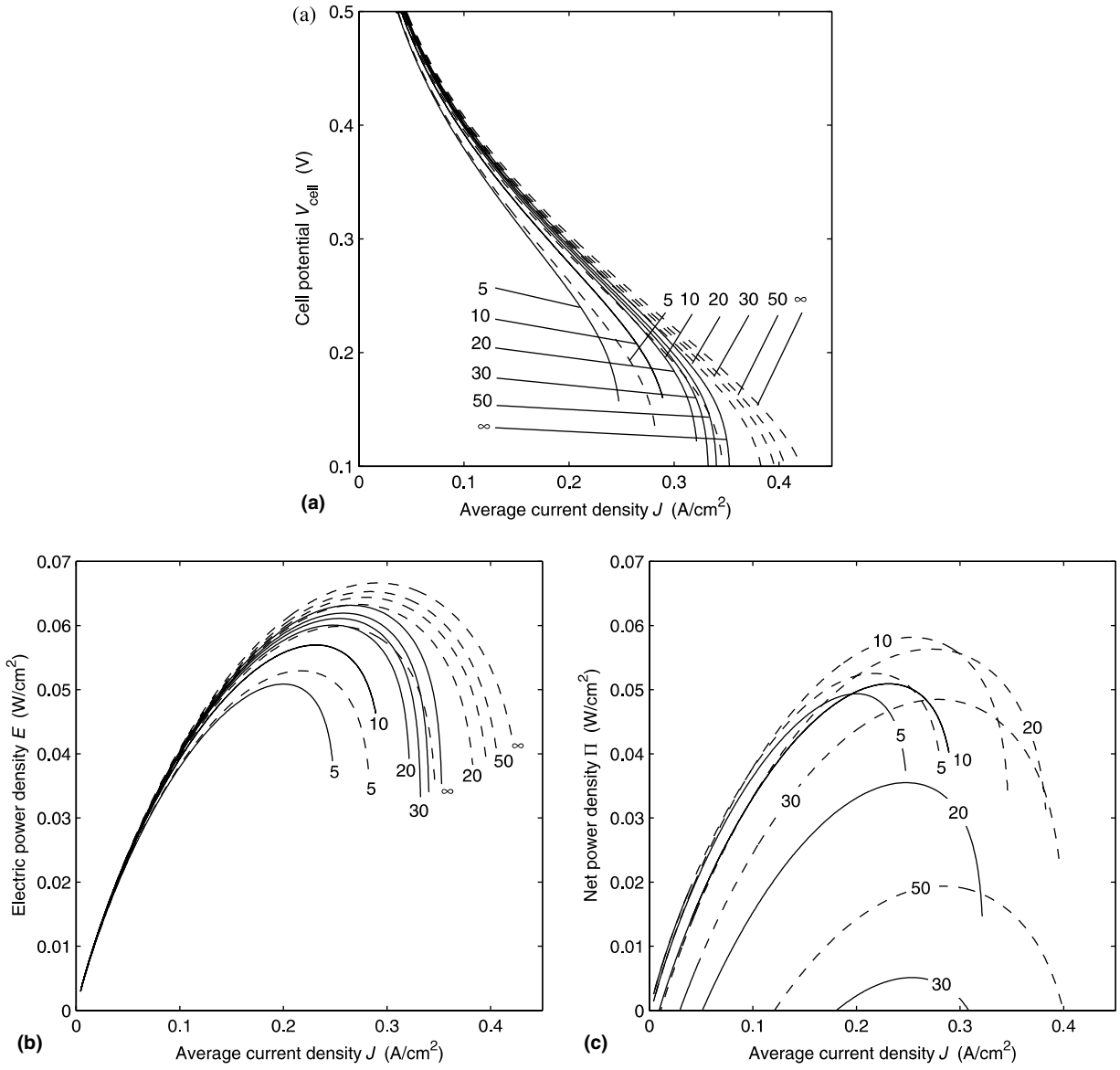

Fig. 6. Performance of a cell with a traditional fluid distributor (solid lines) and a cell with a tree network fluid distributor (dashed lines) for different inlet velocities v_0^a and v_0^c [i.e., $v_0^a = (0.02, 0.04, 0.08, 0.12, 0.2, \infty)$ m/s and $v_0^c = (5, 10, 20, 30, 50, \infty)$ m/s] for $b_0 = 0.1$ cm, $h_0 = 0.05$ cm, $n = 6$, $\varphi = 2^{-1/3}$, $\phi = 2^{-1/3}$, and $\chi = 6$. Labels indicate values of v_0^c where $v_0^a = 0.02v_0^c/5$. (a) Polarization curves, (b) electric power density curves, and (c) net power density curves.

current density, which together provide a maximum net power density. This maximum can be obtained from the maximum of the envelope enclosing the continuous set of constant velocity curves in Fig. 6(c). The same holds for the traditional fluid distribution system. Note that the maximum electric power density is simply obtained from the maximum of the curve for which the inlet flow rates tend to infinity (see Fig. 6(b)).

The maxima of such envelopes are plotted in Fig. 8 for different inlet channel diameters h_0 and different numbers of branching levels n. In Fig. 8(a), absolute values are plotted for the electric power density and the net power density. In Fig. 8(b), these absolute values are scaled with the corresponding values of a traditional non-bifurcating channel, to compare the two flow distribution systems. From Fig. 8(a), it can be seen that the higher the number of branching levels, the higher the electric power density is, and the same holds for the net power density. The net power density increases for increasing inlet channel diameters h_0 due to a reduced pressure drop. In contrast, the electric power density decreases for increasing channel diameters due to enhanced resistances to mass transfer. The graphs suggest that in trying to maximize the net power density, the number of branching levels must be maximized and the inlet channel diameter must correspond to the higher bound of the parameter range considered here. A finite inlet channel diameter range of practical interest is discussed. If the higher bound of the inlet channel diameter range in Fig. 8(a) and (b) is extended towards higher values, the net power density curves in Fig. 8(a) are

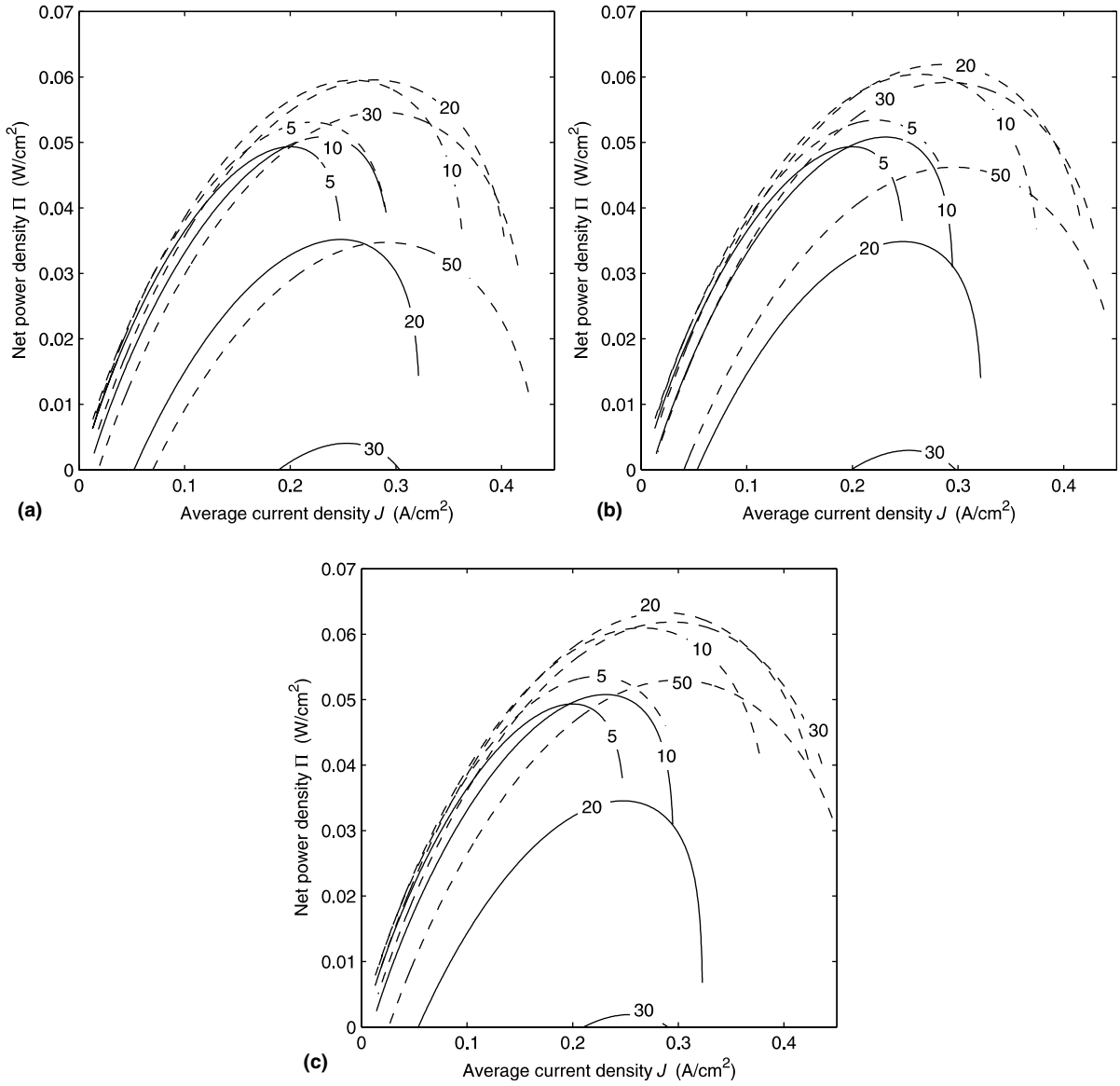

Fig. 7. Performance of a cell with a traditional fluid distributor (solid lines) and a cell with a tree network fluid distributor (dashed lines) for different inlet velocities v_0^a and v_0^c [i.e., $v_0^a = (0.02, 0.04, 0.08, 0.12, 0.2)$ m/s and $v_0^c = (5, 10, 20, 30, 50)$ m/s] with $b_0 = 0.1$ cm, $h_0 = 0.05$ cm, $\varphi = 2^{-1/3}$, $\phi = 2^{-1/3}$, and $\chi = n$. Labels indicate values of v_0^c where $v_0^a = 0.02v_0^c/5$. (a) Net power density curves for $n = 9$. (b) Net power density curves for $n = 12$. (c) Net power density curves for $n = 15$.

expected to have a maximum and the scaled net power density curves in Fig. 8(b) are expected to have a minimum, since the electric power density is monotonically decreasing for increasing inlet channel diameters. The number of branching levels is limited by a manufacturing constraint; that is, there exists a maximum number of branching levels that can be manufactured onto a plate of finite size, although with today's MEMS techniques [18] channels of diameters as small as of the order of 100 nm do not present particular manufacturing challenges. For a tree network with $n = 6$, it is seen from Fig. 8(a) and (b) that compared to the traditional system with $n = 0$ and $\chi = 6$, the tree network system provides 30%, 17%, and 14% higher maximum net power densities for inlet channel diameters h_0 of 0.03, 0.04, and 0.05 cm, respectively. For a tree network with $n = 12$, it is seen that compared to the traditional system with $n = 0$ and $\chi = 12$, the tree network system provides 46%, 26%, and 21% higher maximum net power densities for inlet channel diameters h_0 of 0.03, 0.04, and 0.05 cm, respectively.

It should be noted that the effect of bubbles on the anode side was neglected in this study. In cases where it occurs, the formation of bubbles is expected to increase the volumetric flow rate in the channel, according to conservation of mass. The presence of bubbles will also affect friction, in particular at high void fractions. In addition, the dynamic wetting behavior between the liquid phase, the gaseous phase, and the solid phase of the wall or the porous channel/backing layer interface will play a role in this context, especially for the smaller channels of the

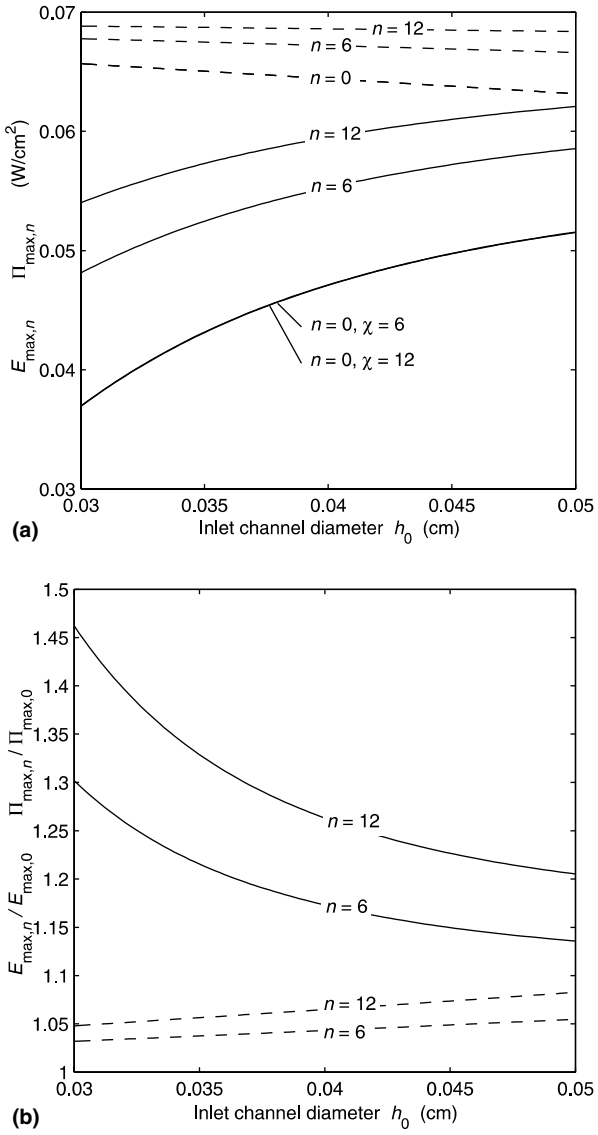

Fig. 8. Maximum electric power density (dashed lines) and maximum net power density (solid lines) based on $b_0 = 2h_0$, $\varphi = 2^{-1/3}$, $\phi = 2^{-1/3}$, and $v_0^a = 0.02v_0^c/5$. (a) Absolute values for the tree network system ($n > 0$) and the traditional system ($n = 0$). (b) Values for the tree network system ($n > 0$) are scaled with the corresponding values of the traditional system ($n = 0$).

higher branching levels. In the smaller channels, the pressure differences between the gaseous and liquid phases may not be negligible. Furthermore, different two-phase flow regimes are to be expected within the proposed tree network channel system containing multiple length scales.

5. Conclusions

Pyramidal direct methanol fuel cells were designed from tree network distribution channels. In contrast to the traditional a priori imposed rectangular shapes of fuel cells, the resulting pyramidal shape of the fuel cell is based on the functionality of the fluid distribution system. A one-dimensional across-the-cell model was utilized and extended in this study to a two-dimensional model to quantify the proposed concept. The current–voltage behavior was predicted for both flow distribution systems and it was shown that it is imperative that the pressure drop and the related pumping power be considered as a loss mechanism when optimizing the fuel cell with respect to maximum net power densities. It was found that tree network channels can provide substantially improved electric and net power densities compared to the traditional non-bifurcating serpentine channels, due to reduced mass transfer resistance between the channel and the channel/backing layer interface, reduced mass transfer resistance in the lateral direction of the backing layer, and reduced pressure drop and pumping power. The influence of the variation of geometric and operating parameters on the electric and net power density were discussed and optima identified. It was shown that tree network channels on pyramidal shaped plates have the potential to significantly improve the performance of direct methanol fuel cells due to their intrinsic advantage with respect to both mass transfer and pressure drop.

Acknowledgement

This work was supported by the Swiss Federal Office of Energy (BFE) under contract no. 87100 (program manager Dr. A. Hintermann).

References

[1] A. Bejan, Shape and Structure, from Engineering to Nature, Cambridge University Press, Cambridge, 2000.
[2] A. Bejan, From heat transfer principles to shape and structure in nature: constructal theory, ASME J. Heat Transfer 122 (2000) 430–449.
[3] A. Bejan, The tree of convective heat streams: its thermal insulation function and the predicted 3/4-power relation between body heat loss and body size, Int. J. Heat Mass Transfer 44 (2001) 699–704.
[4] S.M. Senn, D. Poulikakos, Polymer electrolyte fuel cells with porous materials as fluid distributors and comparisons with traditional channeled systems, ASME J. Heat Transfer 126 (2004) 410–418.
[5] S.M. Senn, D. Poulikakos, Tree network channels as fluid distributors constructing double-staircase polymer electrolyte fuel cells, J. Appl. Phys. 96 (2004) 842–852.
[6] S.M. Senn, D. Poulikakos, Laminar mixing, heat transfer and pressure drop in tree-like microchannel nets and their application for thermal management in polymer electrolyte fuel cells, J. Power Sources 130 (2004) 178–191.
[7] J.V.C. Vargas, A. Bejan, Thermodynamic optimization of internal structure in a fuel cell, Int. J. Energy Res. 28 (2004) 319–339.
[8] A. Bejan, Entropy generation minimization: the new thermodynamics of finite-size devices and finite-time processes, J. Appl. Phys. 79 (1996) 1191–1218.
[9] A.A. Kulikovsky, The voltage–current curve of a direct methanol fuel cell: "exact" and fitting equations, Electrochem. Commun 4 (2002) 939–946.
[10] A.A. Kulikovsky, Performance of catalyst layers of polymer electrolyte fuel cells: exact solutions, Electrochem. Commun. 4 (2002) 318–323.
[11] J.H. Nam, M. Kaviany, Effective diffusivity and water-saturation distribution in single- and two-layer PEMFC diffusion medium, Int. J. Heat Mass Transfer 46 (2003) 4595–4611.
[12] L.X. You, H.T. Liu, A two-phase flow and transport model for the cathode of PEM fuel cells, Int. J. Heat Mass Transfer 45 (2002) 2277–2287.

[13] S. Kakac, R.K. Shah, W. Aung, Handbook of Single-Phase Convective Heat Transfer, Wiley, New York, 1987.
[14] R.B. Bird, W.E. Stewart, E.N. Lightfoot, Transport Phenomena, Wiley, New York, 1960.
[15] E.L. Cussler, Diffusion Mass Transfer in Fluid Systems, Cambridge University Press, Cambridge, 1997.
[16] G. Dagan, Flow and Transport in Porous Formations, Springer, Berlin, 1989.
[17] J. Bear, Y. Bachmat, Introduction to Modeling of Transport Phenomena in Porous Media, Kluwer, Dordrecht, 1990.
[18] T.J. Yen, N. Fang, X. Zhang, G.Q. Lu, C.Y. Wang, A micro methanol fuel cell operating at near room temperature, Appl. Phys. Lett. 83 (2003) 4056–4058.
[19] D.R. Lide, CRC Handbook of Chemistry and Physics, CRC Press, Boca Raton, 1993.
[20] I.E. Idelchik, Handbook of Hydrodynamic Resistance, Hemisphere, New York, 1986.
[21] K. Sundmacher, T. Schultz, S. Zhou, K. Scott, M. Ginkel, E.D. Gilles, Dynamics of the direct methanol fuel cell (DMFC): experiments and model-based analysis, Chem. Eng. Sci. 56 (2001) 333–341.